Scaling of the Ionization Fraction in a Self-Field MPD Thruster

IEPC-2022-605

Presented at the 37th International Electric Propulsion Conference
Massachusetts Institute of Technology, Cambridge, MA, USA
June 19-23, 2022

Edgar Choueiri[1] and Francesco di Lauro[2]
Electric Propulsion and Plasma Dynamics Laboratory, Princeton University, Princeton, NJ 08540, USA

Using spectroscopic measurements of ArI and ArII line intensities in the discharge chamber of a steady-state self-field magnetoplasmadynamic thruster (MPDT) operated over a wide range of operation conditions, it is shown that the axial profiles of the ionization fraction α in the chamber scales with a similarity parameter ξ (the "MPDT scaling number"), which combines the operation parameters in a non-dimensional number, and was found previously to be a fundamental parameter scaling many aspects of MPDT performance. The ionization fraction at a given axial location within a large upstream portion of the chamber was found to exhibit a linear scaling with ξ irrespective of the dimensional operation parameters. The scaling reveals a distinct transition between two modes of operation, $\xi \leq 1$ and $\xi > 1$. This transition, and the flattening of the axial profiles of α at a high value as ξ nears 1, suggest that by raising ξ through 1 the thruster transitions from a mode where the acceleration and ionization power sinks are competing, to a more efficient mode where the ionization sink is largely saturated, thus allowing the acceleration power to increase more vigorously with input power.

I. Introduction

Ionization in MPD thrusters[a] (MPDTs) has long been known to be a significant power sink, whose magnitude, at nominal thruster operation conditions, is of the same order as that of the power associated with acceleration [1]. Detailed spectroscopic measurements [2] have shown that less than 10% of the power tied in ionization is recovered in the exhaust, and that as much as 85% of the internal energy is in ionization. Therefore, an understanding of the scaling of ionization as a function of operation conditions is necessary for obtaining accurate models of MPDT thrust efficiency.

There have been a few theoretical studies of ionization in MPDTs covering aspects such as nonequilibrium effects[3, 4], ionization rates[5], and pre-ionization[6] but, mostly due to the difficulty of obtaining optical access to the ionization region in the inter-electrode region of the MPDT, there has been only one published detailed experimental study, by Randolph et al [7–9], focusing on ionization. In that study, a thruster with an axial optical window was used to carry out line emission spectroscopic measurements that provided the first quantitative picture of the axial profile of the ionization fraction inside the thruster. The study also confirmed that vigorous ionization of the injected neutral propellant in an MPDT occurs abruptly far upstream in the discharge region through a thin (with an axial extent of a few mm) shock-like layer, called the ionization front. The existence of such a front was previously reported in 1968 in a single sentence[b] in a brief paper by Abromov et al. [10]. Sheppard and Martinez-Sanchez proposed a classical mechanism of "back diffusion" of charged particles near the gas inlet to explain the thinness of the ionization region, while Choueiri and Randolph [11], in light of theoretical and experimental evidence of the existence of current-driven microinstabilities [12–15] in the MPDT plasma, used a parametric electron energy distribution that allows for suprathermal electrons to model the extent of the ionization front, and argued that the small axial extent of that front is consistent with ionization by electrons "anomalously" heated through microturbulence.

[1]Professor, Electric Propulsion and Plasma Dynamics Laboratory, Princeton University, choueiri@princeton.edu
[2]Graduate Student, University of Pisa; Visiting Student Research Collaborator, Princeton University, frn.dilauro@gmail.com

[a]This study is focused on the self-field variant of the MPDT. Throughout this paper, the term MPDT refers to that variant.

[b]Commenting on a figure showing their axially resolved measured of ion emission, the authors of Ref. [10] stated "It is interesting to note that the intensity of the ionic lines shows a sharp jump at the entrance of the discharge region, which indicates the presence of a narrow ionization front." They also briefly speculated that this front may be related to the existence of suprathermal electrons in that region.

Given the importance of the power locked in ionization to the power sink partitioning regulating the thrust efficiency of the MPDT, a more practical question is how the ionization fraction, and its evolution along the acceleration region, scale with the operation parameters. Such a scaling, if cast in terms of the same non-dimensional scaling parameter that is known to scale other power sinks, would be useful for arriving at a universal model for the efficiency of MPDT thrusters.

Several experimental studies have shown that the dimensionless parameter ξ, which we refer to as the "MPDT scaling number," is a fundamental scaling parameter for MPD thrusters. Indeed, it has been shown that ξ scales many aspects of MPDT performance, such as voltage [16], thrust [17], erosion [18], discharge symmetry [19], and anode drop [20]. In particular, Choueiri, in 1998 derived a semi-empirical MPDT thrust model using ξ as the scaling parameter [21].

The MPDT scaling number (whose derivation was first given [21], and which we summarize here for convenience) is tied to the concept of *nominal operation*, which is the operation point at which the directed kinetic power in the exhaust (which is associated with thrust) is equal to the power in the ionization sink when the entire mass flow rate is at the first ionization potential, ϵ_i[21]:

$$\frac{1}{2}Tu_{ex} = \dot{m}\frac{\epsilon_i}{M}. \tag{1}$$

Here T is the thrust, $\dot{m}$ is the mass flow rate, u_{ex} is the exhaust speed, M is the atomic mass, and ϵ_i is the first ionization potential. Making the justifiable[2] approximation that thrust in the MPDT is dominated by its electromagnetic component, we have $T = bJ^2$, $u_{ex} = T/\dot{m} = bJ^2/\dot{m}$, where, to a good approximation, $b = (\mu_o/4\pi)\ln(r_a/r_c)$ is a parameter that depends on the thruster geometry and represents its inductance per unit length. The above power equipartition, which defines nominal thruster operation, leads to

$$\left(\frac{\mu_o}{4\pi}\ln\frac{r_a}{r_c}\right)^2 J^4 = \dot{m}^2 u_{ci}^2, \tag{2}$$

where u_{ci} is defined as

$$u_{ci} \equiv \left(\frac{2\epsilon_i}{M}\right)^{1/2}, \tag{3}$$

and is known as the critical ionization velocity. For xenon, argon and lithium, u_{ci} is 4.22, 8.72 and 12.24 km/s, respectively. The current at which the nominal operation condition is reached is called the critical ionization current, J_{ci}. From the above equation we have,

$$J_{ci} = \left(\frac{\dot{m}u_{ci}}{b}\right)^{1/2}. \tag{4}$$

This characteristic current is used to normalize the total current leading us to the dimensionless parameter ξ, which we referred to above as the "MPDT scaling number":

$$\xi \equiv \frac{J}{J_{ci}}. \tag{5}$$

More explicitly in terms of the controllable parameters of thruster operation,

$$\xi = J/\left[\frac{\dot{m}^{1/2}\,(2\epsilon_i/M)^{1/4}}{\left(\frac{\mu_o}{4\pi}\ln\frac{r_a}{r_c}\right)^{1/2}}\right]. \tag{6}$$

When the MPDT scaling number is equal to unity, the thruster is said to be at its nominal operation condition, with a nominal specific impulse $I_{sp} = u_{ci}/g_o$, irrespective of the input power level.

The main three questions we wish to address in this paper are

- Q1: Is ξ a valid scaling parameter for α?
- Q2: If ξ is a valid scaling parameter for α, is the scaling linear or nonlinear?
- Q3: To what extent is that scaling valid, and what are its implications?

Randolph et al. [7] stated that they found the ionization fraction to have "a strong scaling with $J^2/\dot{m}$". This implies a scaling with ξ^2 (given that all their measurements were done with the same thruster, therefore fixed r_a/r_c, and the same propellant, therefore fixed m_i and ϵ_i). However, the only evidence they provide in support of this statement is a plot showing that two ionization axial profiles, taken at two different operation points (J_1,$\dot{m}_1$) and (J_2,$\dot{m}_2$), but having the same value of J^2,$\dot{m}$, coincide.

Two operation points are neither enough to establish the existence of such a scaling, nor to verify that the scaling goes as $J^2/\dot{m}$ (i.e. ξ^2). Indeed, as we shall see after we analyze the same experimental data more extensively, the ionization fraction is found to scale with $J/\sqrt{\dot{m}}$, and therefore the scaling is linear, and not quadratic, with ξ.

To address the questions we posed above, we started with the existing raw measurements of the relative line intensities data for ArII and ArI that was processed by Randolph [9] from photographs of the emission spectra. The spectroscopic measurements were obtained through an axial optical window of a 20 kW-class MPDT over a wide range of currents and mass flow rates. We reduced the data following the same procedure described in that reference, and summarized in the Appendix, (i.e. assuming a non-equilibrium and optically thin plasma, under the corona model approximation) to obtain axial profiles of the ionization fraction α along the thruster's axis. We then statistically analyzed the dependence of α on ξ to reveal and characterize the scaling.

II. Experimental Setup

A. Thruster and facilities

The MPD thruster used in Randolph's experiments, on which our study is based, was derived from the design of the Princeton 20 kW class thruster [22, 23]. A schematic drawing is shown in Fig. 1. The thruster consists of a cylindrical graphite anode with an exit diameter of 3.5 cm and a thoriated tungsten cathode rod with a diameter of 0.64 cm and a length of 7 cm. This thruster was modified with a 3 mm wide radial slot that was machined from the interior surface of the insulator to the exterior surface of the graphite anode body. This slot was 7 cm in length along the thruster's axis, and extended from the propellant inlet port to the thruster exit plane, thus allowing optical access to the entire inter-electrode region (see right panel of Fig. 1). A quartz window, secured by a ceramic holder, was used to prevent the propellant from flowing out. A fiberglass thread was used, instead, to secure the ceramic holder and provide a well-defined axial geometric reference on all spectra. Typical operation conditions for this thruster were:

- thruster current, J: 50 A to 900 A;
- terminal voltage, V: 15 V to 50 V;
- mass flow rate, $\dot{m}$: 3 mg/s to 11 mg/s.

Randolph's experiments were conducted using argon as propellant in the steady-state MPDT facility of Princeton University which consists of a large 6.4 m long steel vacuum tank with a diameter of 1.5 m. Vacuum was maintained below 5×10^{-4} Torr by a 1.2 m-diameter diffusion pump backed by a mechanical pumping system.

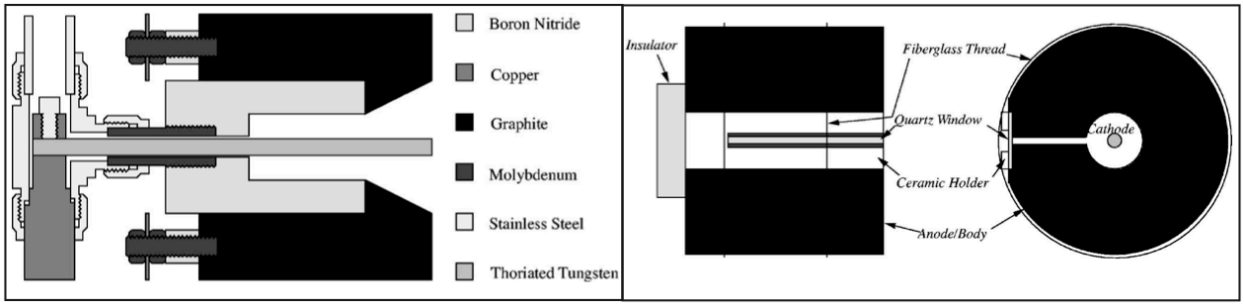

Fig. 1 Schematic drawing of the thruster. The right panel shows the side and front views of the radial slot used for optical access to the plasma in the discharge chamber. From Ref. [9].

B. Diagnostics

A schematic of the optical system used by Randolph is shown in Fig. 2. Light emitted from the inter-electrode region passes through a quartz window in the vacuum chamber and is collected by an achromatic lens. A mirror reflects

the emitted light through a dove prism which was used to rotate the horizontal image of the thruster slot to align it with the 2 cm tall vertical spectrometer entrance slit. A 0.75 m Czerny-Turner spectrometer was used to measure the emitted light. The resulting spectra were recorded on a Polaroid 57 film by a manually triggered shutter. The axial coordinate for plotting the profiles of α is shown schematically in Fig. 3, along with sample axial profiles of ArI and ArII line intensities.

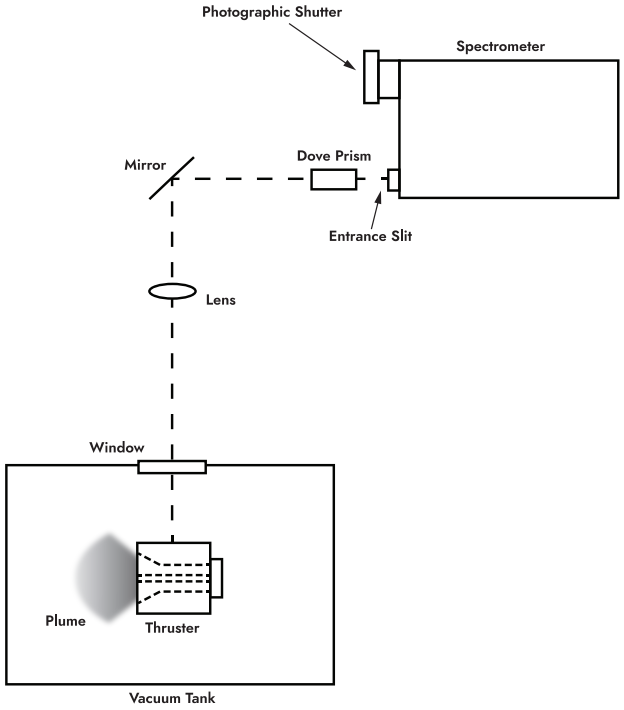

Fig. 2 Schematic of the experimental setup. From Ref. [9].

III. Analysis and Results

Following the procedure described in the appendix, we were able to reproduce Randolph's evaluation of the electron temperature, which ranged between 1 and 1.2 eV. We then calculated the ion-neutral number density ratio with Eq. 13 using an ArI (4259 Å) emission line and one for ArII (4014 Å). This allowed us to calculate the ionization fraction, α:

$$\alpha = \frac{N_1^+}{N_1}\left(1 + \frac{N_1^+}{N_1}\right)^{-1}. \tag{7}$$

An example of the raw relative intensity profiles of relevant emission lines is shown in the right panel of Fig. 3. The lack of data in the region marked in grey in that figure is due to a fiberglass thread, used to secure the quartz window to the thruster body, blocking optical access.

The two primary sources of error are related to the measurement of the electron temperature via Eq. 14. The first source of error is associated with the uncertainties in the Einstein coefficients. Such errors, however, only affect the absolute value of the electron temperature. The second source of error is related to the values of the relative intensities of the emission lines and is caused by the bit resolution of the scanner used to digitize the photographs obtained with the spectrometer. This is the most significant source of error and was therefore used to calculate the error bars of the figures of this section. The same error sources affect the ion/neutral number ratio measurements. However, the uncertainty here is much larger due to the exponential dependence on the electron temperature in Eq. 13. As a result, confidence in the absolute values of the ion-neutral ratio is good within an order of magnitude. Nonetheless, relative comparison of the ionization fraction for different thruster operation conditions or different axial positions, which is our aim, is largely immune from this uncertainty.

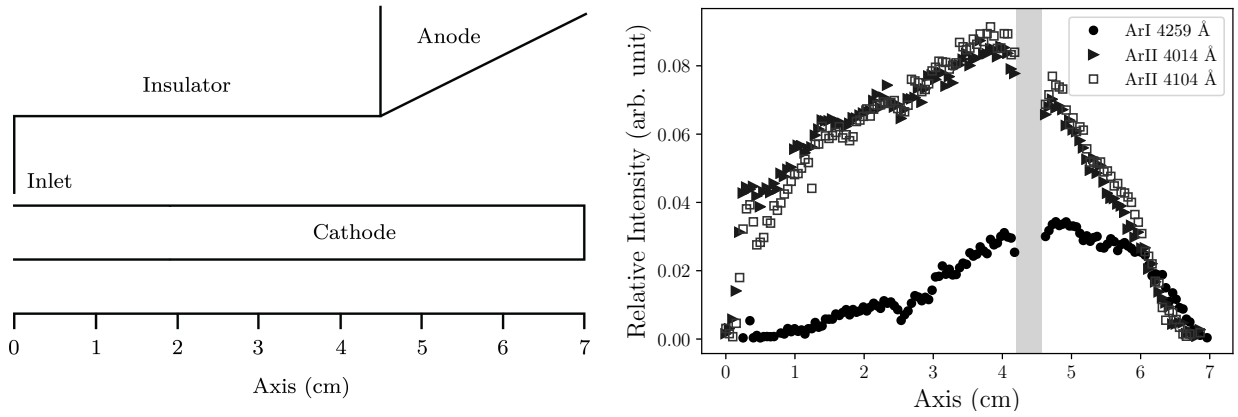

Fig. 3 Thruster chamber geometry and x-coordinate axis. (In the plots of the axial profile of α the axial coordinate is normalized as $\bar{x} = x/lc$, where $l_c = 7$ cm is the cathode length.) The right panel shows sample relative line intensity profiles at $\dot{m} = 5.5$ mg/s and $J = 280$ A. (The lack of data in the grey region is due to a fiberglass thread, used to secure the quartz window to the thruster body, blocking optical access.)

A. Scaling of the ionization fraction profile with ξ

Profiles of the ionization fraction α as a function of the normalized axial position $\bar{x}$, for a range of operation conditions are shown in Fig 4 for four values of ξ. It is important to note, from all the profiles in this figure, the existence of a thin ionization front near $\bar{x} = 0$ where the ionization level of the injected propellant goes from zero to its (generally) highest value ($\alpha > 0.9$) in the profile, over a very short distance compared to the size of the discharge. This was found to be case, not only for the 8 operation conditions covered in these 4 plots, but also for all operating conditions for which we have data. This suggests that the ionization front is a fundamental feature of ionization in the MPDT.

Of more relevance to the questions we posed above, is the clear qualitative and quantitative scaling of the α profiles with ξ. We first note that the ionization fraction, up to least $\bar{x} \simeq 6$, does not depend on the operation condition (i.e. the dimensional values of J and $\dot{m}$) but rather on the non-dimensional scaling parameter ξ. This provides the first evidence that ξ is a relevant similarity parameter.

Furthermore, we note that even the qualitative aspect of the α profiles is controlled by ξ: At low values of ξ the profiles show a significantly drooping profile, with α dropping downstream by as much as 40% from its value at the ionization front[c]. Increasing ξ, irrespective of the dimensional operation parameters, has the remarkable effect of significantly flattening the axial profiles, which, for $\xi = 1$ become essentially flat, maintaining the high ionization fraction of the ionization front, over a large axial extent of the discharge chamber.

Increasing ξ beyond 1, even by more than 50%, has little qualitative and quantitative effects on the profile, which remains flat at essentially the same high value of α attained at the ionization front, as we see from the $\xi = 1.56$ plot of Fig, 4. This suggests that $\xi \simeq 1$ represents a saturation condition for ionization.

B. Scaling of the local ionization fraction with ξ

To gain further insight into the nature of the scaling of α with ξ we examined how the local values of the ionization fraction (i.e. at fixed values of $\bar{x}$) depend on the MPDT scaling parameter.

The upper half of Fig. 5 shows the typical case of a location near the center of the chamber ($\bar{x} = 0.53$), where in the left plot, α is plotted as a function of J for 4 values of $\dot{m}$, and as a function of ξ in the right plot. We note the significant scatter of data in the left plot, where the data is plotted versus the dimensional parameter J. A hallmark of a relevant scaling parameter is its ability to significantly reduce the y-axis scatter of the same data when that parameter is used as the x-axis coordinate, and collapse the data over a curve whose functional dependence (e.g. linear, non-linear) can be discerned.

Such data scatter collapse is clearly seen in the top right plot of 5, with the exception of three data points. The

[c]We caution against interpreting the decay of the α with $\bar{x}$, at low values of ξ, as a sure sign of recombination, as the ion density (a measure of which we do not have, since the relative line intensity method yields a measure of the ratio N_1^+/N_1 and not N^+) may well be decreasing much faster than the neutral density due to the ion being convected away through plasma acceleration, and the neutrals staying behind due to the weak momentum coupling with the ions at the typically low densities of the MPDT plasma.

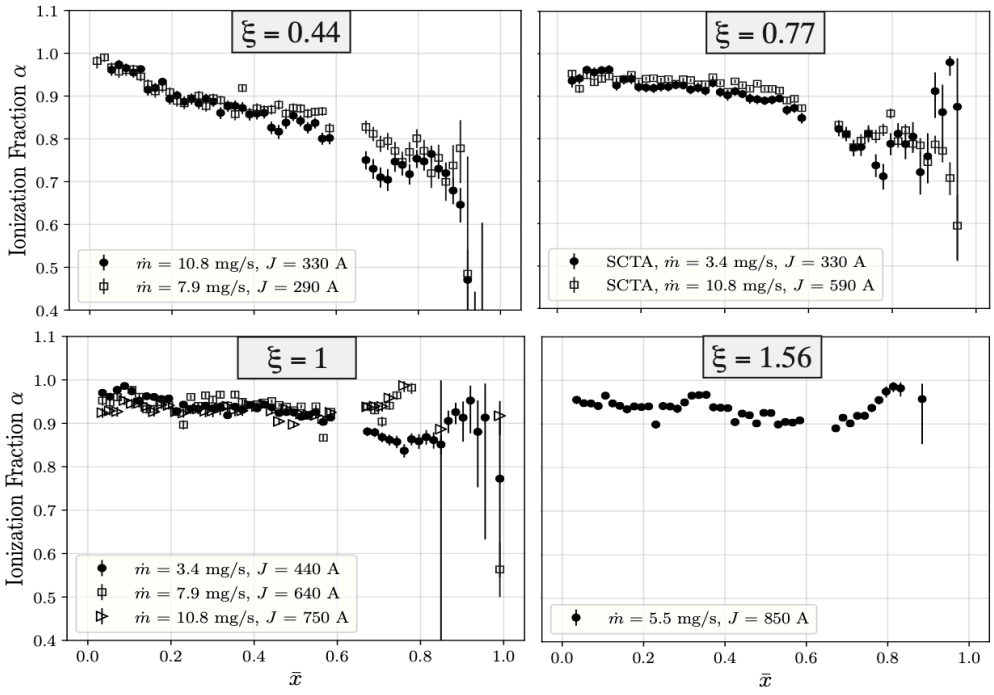

Fig. 4 Ionization fraction profiles plotted as a function of the normalized channel length $\bar{x}$ for four values of ξ.

first one is at $\xi = 1.23$, and its departure from the observed ξ scaling can be attributed to operation ($\xi > 1$) near the so-called "onset" condition [24], where enhanced erosion[25] may be expected to alter the argon ionization process, and to cause the effective value of $\dot{m}$ to be different than that of the injected propellant mass flow rate used to calculate ξ. The other two data points, at $\xi = 0.56$ and 0.43, are outliers. The first, and the one with the most departure in scaling, is singular for being at the lowest current for the lowest mass flow rate investigated (3.4 mg/s), and may reflect a limit for the validity domain of the scaling (question Q3). Still, the fact that the spread in the remaining 13 data points clearly collapses unto a curve gives further support to the claim that ξ is a scaling parameter for α (question Q1).

The bottom plots of Fig. 5 show the case of an axial position further downstream ($\bar{x} = 0.7$). Here, the collapse and the linear dependency are less pronounced, but still evident. This indicates that the linear scaling with ξ becomes tenuous as we go too far downstream from the ionization front. Indeed, similar plots of α vs ξ for $\bar{x}$ varying from 0.14 to 0.81, allow us to make the following observations:

1) The collapse of the scatter in the data, indicating good scaling with ξ, is quite evident up to about $\bar{x} \simeq 0.8$. With increasing distance from the inlet (and thus the ionization front) the scatter progressively increases, and a linear fit (up to $\xi = 1$) becomes worse.
2) With increasing distance from the ionization front, the slope of the linear fit goes from near zero at $\bar{x} \leq 0.37$ (with all values of α close to 1 and with little scatter) to as high as near unity for $\bar{x} = 0.8$, downstream of which which the linear scaling with ξ becomes tenuous due to the data scatter.
3) In all cases where a linear scaling can be discerned ($\bar{x} \leq 0.8$) it stops abruptly when ξ starts exceeding unity.

C. Evidence of two operation modes

Although we have relatively limited data at $\xi > 1$ (where it becomes difficult to operate the thruster due to the "onset" condition) the abrupt termination of the linear $\alpha(\xi)$ scaling when ξ starts exceeding unity, suggests that there exist two operation modes defined by $\xi \leq 1$, and $\xi > 1$.

To better discern these two operation modes, we analyzed the data using a simple linear regression approach. Starting with a linear fit that uses the first two data points in the α vs ξ plot, then adding the data point for the next value of ξ, calculating the goodness of the linear fit, R^2, and repeating for the rest of the data set, we generated plots of the the variation of R^2 as a function of ξ for a wide range of axial locations.

The existence of the two modes would then be manifested by a peak in the plot of R^2 vs ξ near $\xi = 1$, followed by a

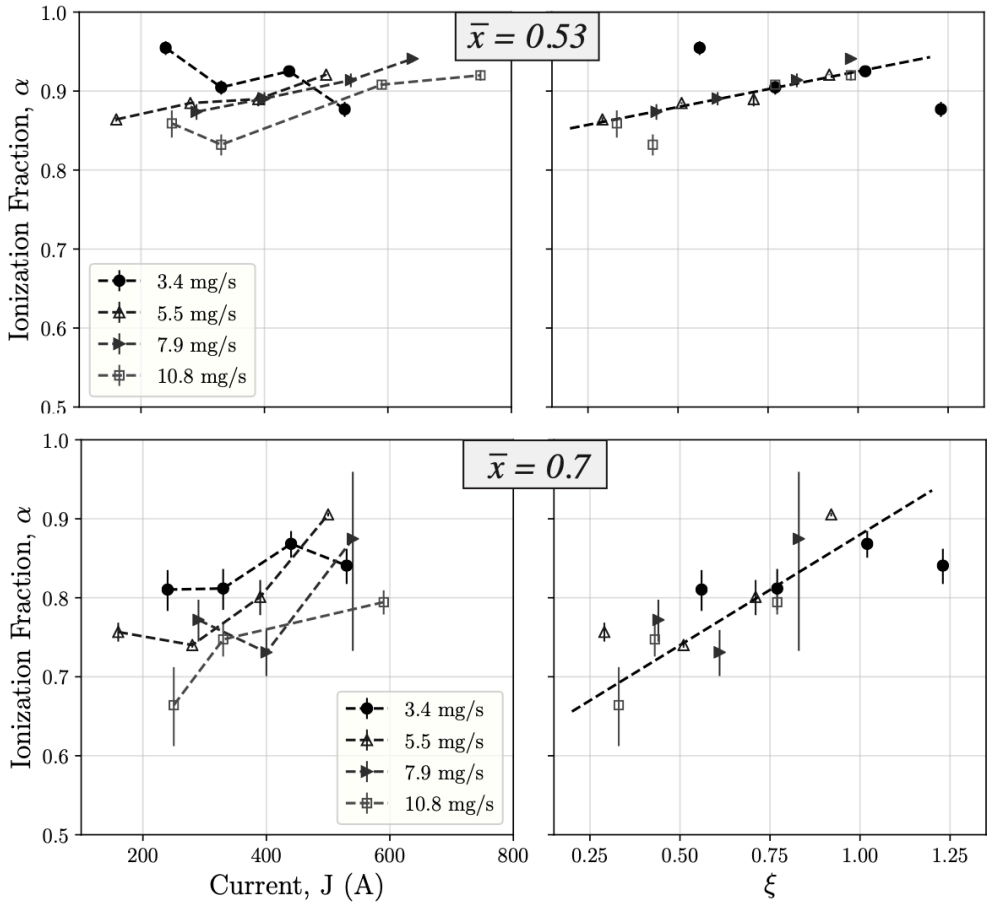

Fig. 5 Scaling of α as a function of J (left) and ξ (right) at $\bar{x} = 0.53$ (top) and 0.7 (bottom) for four values of the argon mass flow rate. (The linear fits exclude the data points for $\xi > 1$ and the upper fit,, excludes the two outliers, $\xi = 0.43$ and 0.56.)

sharp decrease of R^2. This is indeed seen in Fig. 6, for the typical mid-cathode case of $\bar{x} = 0.53$.

Since the extent of the data at $\xi > 1$ is limited, we have repeated the analysis for different axial positions and calculated the spatially-averaged value of R^2 over the upstream and downstream regions of the chamber. In Fig. 7a we show a plot of R^2 vs ξ, spatially averaged over the upstream axial region $\bar{x} = 0.3 - 0.57$, which is sufficiently far from the ionization front at the inlet port where the ionization fraction is more insensitive to changes in the mass flow rate. The existence of the two modes, reflected by the peak is still evident. The same holds for the downstream region $\bar{x} = 0.7 - 0.84$ as seen in the (Fig. 7b) where the peak in R^2 is clear.

IV. Summary and Discussion

We first summarize the main findings of our study, then discuss some of their implications.

1) Axial profiles of the ionization fraction inside the discharge chamber of a 20-kW-class self-field MPDT, measured over a wide range of operation parameters, exhibit a remarkably pronounced scaling with the MPDT scaling parameter, ξ.
2) With increasing ξ the high ionization fraction attained at the ionization front (robustly located at the every beginning of the current conduction region) is maintained throughout an increasingly large axial region downstream of the front.
3) When ξ reaches 1 the axial profile of the ionization fraction becomes essentially flat, and remains so with further increase in ξ.
4) Over a large axial extent of the thruster's chamber, the *local* value of the ionization fraction scales with ξ

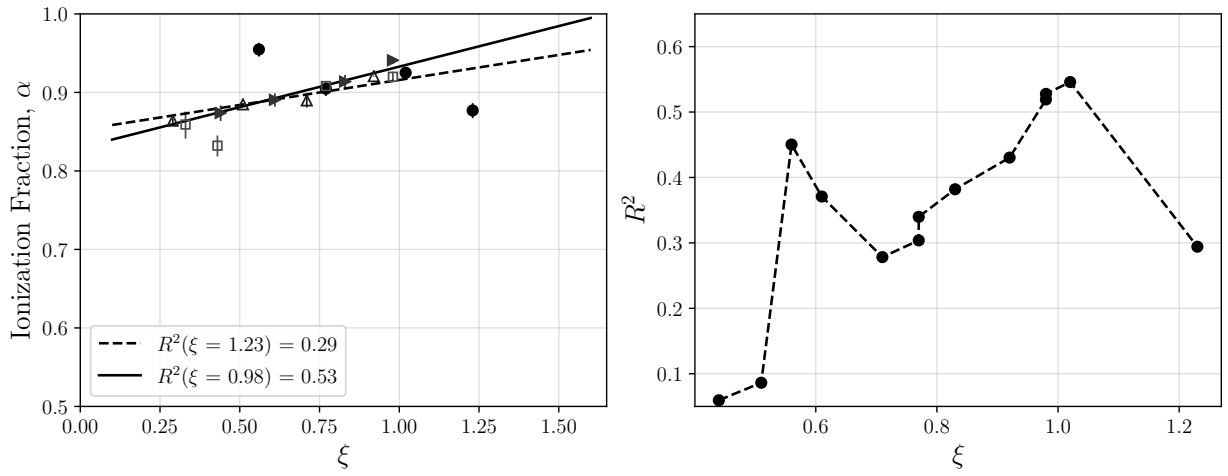

Fig. 6 Variation of R^2, at an axial location $\bar{x} = 0.53$, obtained by increasing the number of data points used for the linear regression analysis.

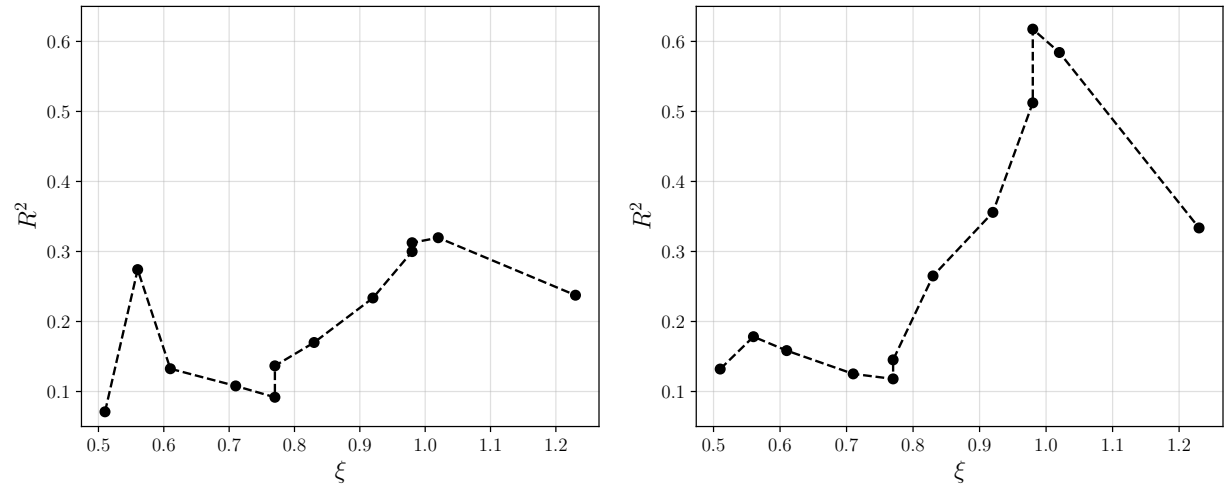

(a) $\bar{x} = 0.3 - 0.6$ (b) $\bar{x} = 0.7 - 0.84$

Fig. 7 Average of the variation of R^2 vs ξ, over two axial regions.

irrespective of the dimensional operation parameters, up to $\xi \simeq 1$, above which the scaling is disrupted.

5) The scaling of $\alpha(\bar{x})$ with ξ is linear (i.e. $\propto J/\sqrt{\dot{m}}$, and not $J^2/\dot{m}$ as perviously [7] surmised.
6) Both the flattening of axial profiles of α when $\xi \geq 1$ (Finding 2) and the disruption of the linear scaling of the local value of α when the condition $\xi \simeq 1$ is exceeded (Finding 4), implicate the existence of two qualitatively distinct modes of operation: $\xi \leq 1$, and $\xi > 1$.

The existence of such two MPDT operation modes ($\xi \leq 1$ and $\xi > 1$), found here in the context of ionization, echoes a previous finding [21] that the scaling of thrust in the self-field MPDT also exhibits a bi-modal behavior with $\xi \simeq 1$ as the transition condition. Specifically, the "thrust coefficient", C_T, defined as

$$C_T \equiv \frac{4\pi}{\mu_o}\frac{T}{J^2}, \tag{8}$$

and which is order of unity, and can be measured accurately with a thrust stand and a current probe, was found to obey the following scaling with ξ

$$C_T = \frac{\nu}{\xi^4} + \ln\left(\frac{r_a}{r_c} + \xi^2\right), \tag{9}$$

where ν is a non-dimensional parameter that depends only the mass flow rate and is of order 10^-2. This scaling, which was verified extensively with argon, krypton and xenon propellants, also exhibits a bi-modal, $\xi \leq 1$, and $\xi > 1$, behavior: when $\xi \leq 1$, C_T scales strongly with ξ (due to the ξ^{-4} term) then transitions quickly, with increasing ξ, to a much weaker dependence on ξ (due to the natural log) when the latter exceeds unity.

The fact that C_T varies little as ξ grows from 1 to a value not far from 1 (where "onset phenomena" occur) has direct relevance to the implication of Findings (2) and (4). With C_T essentially constant in Mode 2 ($\xi \geq 1$), $T \propto J^2$, and since $u_e \propto J^2$, the thrust power scales with ξ^4. From Finding (2) we expect that operation in Mode 2 effectively saturates the power sink associated with first-level ionization. This leads to the qualitative picture that the transition from Mode 1 ($\xi \leq 1$) to Mode 2 ($\xi > 1$) is from a mode where ionization and acceleration are competing, to one where the ionization power sink is effectively capped while the acceleration power keeps increasing with ξ^4, leading to enhanced thrust efficiency.

Finally, we note that the scaling of α we found in the experimental data is, strictly speaking, a scaling with the dimensional parameter $J/\sqrt{\dot{m}}$, and not necessarily with ξ, since m_i and ϵ_i were not varied in the experiments whose data we used. However, the fact that the similar mode transition of C_T through $\xi \simeq 1$ has been verified experimentally with various atomic propellants [21] (including argon), and the more telling fact that the mode transition that we found for α occurs clearly when ξ goes through 1 (a singular non-dimensional number marking the power equipartition expressed in Eq. 2, while the corresponding dimensional value for $\propto J/\sqrt{\dot{m}}$ would, by itself, be arbitrary) suggests that the scaling with that particular non-dimensional version of $J/\sqrt{\dot{m}}$, namely ξ, is unlikely to be fortuitous.

Appendix

Since some aspects of the data reduction procedure we followed to generate the data presented in this paper, although discussed in Randolph's masters thesis [9], were not described in the two conference papers (the only publications resulting from that thesis work), we summarize that procedure in this appendix.

Once species had been identified (in the 3900 Å to 4400 Å argon spectral range), photographs were digitized via an electronic scanner with a resolution of 300 dots per inch. Photographic density was reduced to gray level information by an 8-bit analog-digital converter and stored as TIFF image files.

Spectroscopic data obtained in this way have a fine spatial resolution, in the order of 0.2 mm, along the thruster axis. Unfortunately, radial resolution was not high enough to obtain 2-D data. Photographic spectra were so integrated along the thruster axis. Plasma properties away from sheaths are relatively constant through most of this region [26] so that radially integrated measurements are a good representation of the average properties of the inter-electrode plasma.

Once stored as image files, data were further reduced to obtain spectral line intensities. The photographic density data were converted to photographic exposure by a calibrated film characteristic curve. Photographic exposure was then corrected for film wavelength sensitivity by a calibrated wavelength versus sensitivity equation. It is important to note that the photographic exposure is proportional to the film exposure time. However, when relative intensity measurements are made on the same piece of film, as is the case with all quantitative measurements obtained by Randolph, the exposure time factor cancels out. In this way, it was possible to obtain emission line intensity profiles along the thruster axis.

A general way to determine the ionization fraction in non-thermal plasmas by using spectroscopic data is to use a full *collisional-radiative* model that describes the behavior of the plasma by taking into account the rate coefficients of the different processes involved. Following the work of Suckewer [27], in a non-equilibrium plasma the excited state population can be related to the ground state population by means of a modified Boltzmann distribution:

$$N_n = B_n N_1 \frac{g_n}{g_1} \exp\left(-\frac{E_n - E_1}{kT_e}\right), \tag{10}$$

where N_n and N_1 are the number densities of a generic excited state n and ground state 1, respectively; g is the statistical weight of the corresponding state, E is the energy, k the Boltzmann constant, T_e the electron temperature, and B_n is a non-equilibrium coefficient for state n.

In a collisional-radiative model, the coefficient B_n is function of the several excitation rate coefficients that describe the population variations between the different states. The collisional-radiative model is thus an accurate method to

Table 1 Simplified energy model for ArI.

	Level	Energy (eV)	g
1	3p	0	1
2	4s	11.577	8
3	4s′	11.802	4
4	4p	13.096	24
5	4p′	13.319	12
6	3d 5s	14.019	48
7	3d′ 5s′	14.242	24
8	5p	14.509	24
9	5p′	14.690	12

determine the non-equilibrium population distributions of the excited states. However, as it requires the knowledge of all the different rate coefficients, it is quite complex and difficult to apply to spectroscopic measurements.

Nonetheless, Randolph has shown [9] that the *corona model*, which takes its name from its applicability to the solar corona, is a good approximation of the full collisional-radiative model for the electron densities of interest. The assumption of this model is that all upward transitions that populate the excited state n are collisional while all downward transitions that depopulate n are radiative. However, only the ground state 1, because of its dominant population, is important in the collision process. This assumption greatly reduces the complexity of the problem at the expense of some accuracy. With this regard, the non-equilibrium coefficient B_n for the corona model can be expressed as

$$B_n = \frac{N_e K_{n1}}{\sum_{i<n} A_{ni}}, \tag{11}$$

where K_{n1} is the collisional de-excitation rate from state n to ground state 1 while A_{ni} is the transition probability (i.e. the Einstein coefficient related to the spontaneous emission) from state n to a generic lower state i.

In an optically thin plasma, spectral line intensities are directly proportional to the number densities of the excited states [28]. That is:

$$I_{ji} \propto \frac{A_{ji} N_j}{\lambda_{ji}} \tag{12}$$

where I_{ji} is the intensity of the line associated with the transition from a generic upper excited state j to a lower state i, λ_{ji} the corresponding wavelength, A_{ji} the transition probability and N_j the population of the excited upper state j.

Taking the ratio of ion and neutral emission line intensities, and substituting Eq. 10 for the ion and neutral excited state number densities, leads to

$$\frac{N_1^+}{N_1} = \frac{I_{nm}^+ A_{pq} \lambda_{nm}^+ g_1^+ g_p B_p}{I_{pq} A_{nm}^+ \lambda_{pq} g_1 g_n^+ B_n^+} \exp\left(-\frac{E_{n1}^+ - E_{p1}}{kT_e}\right), \tag{13}$$

where subscripts p and q denote the upper excited state and the lower state of neutrals, respectively, and the subscripts n and m denote the upper and lower states of the ions (superscripted with "+")

This way, the dependency from the electron number density N_e, which is unknown, is removed. The line intensities and the wavelengths of the transitions are obtained from the spectroscopic data.

The other parameters, such as excitation rates, transition probabilities and statistical weights, depend on the energy and atomic model adopted. This model was reported by Randolph [9] and related detailed information can be found in Refs. [29–33]. The simplified energy models adopted for both ArI (neutrals) and ArII (ions) are shown in Tables 1 and 2.

For obtaining the electron temperature T_e, the method of relative line intensities, which relies on comparing two ArII transitions [34], is used. The method yields the following expression

$$kT_e = \frac{E_k - E_n}{\ln\left(\frac{I_{kh} A_{nm} \lambda_{kh} g_n}{I_{nm} A_{kh} \lambda_{nm} g_k}\right)}, \tag{14}$$

Table 2 Simplified energy model for ArII.

	Level	Energy (eV)	g
1	$3p^5\ ^2P^0$	0.059	6
2	$3p^6\ ^2S$	13.476	2
3	$3d\ ^4D$	16.420	20
4	$4s\ ^4P$	16.702	12
5	$4s\ ^2P$	17.177	6
6	$3d\ ^4F$	17.688	28
7	$3d\ ^2P$	18.016	6
8	$3d\ ^4P$	18.300	12
9	$4s\ ^2D$	18.438	10
10	$3d\ ^2F$	18.542	14
11	$3d\ ^2D$	18.697	10
12	$4p\ ^4P^0$	19.244	12
13	$4p\ ^4D^0$	19.543	20
14	$4p\ ^2D^0$	19.707	10

which is valid under the assumption of partial local thermodynamic equilibrium (LTE). Indeed, Randolph showed that energy levels above 19 eV for ArII tend to have similar non-equilibrium population deviations with each other. Therefore, even if equilibrium deviations from the ground state may be large, partial LTE is somewhat justified for these excited states.

References

[1] Villani, D., "Energy Loss Mechanisms in a MPD Arcjet," Ph.D. thesis, Princeton University, Princeton, NJ, USA, 1982.

[2] Bruckner, A. P., and Jahn, R. G., "Exhaust Plume Structure in a Quasi-Steady MPD Accelerator," *AIAA Journal*, Vol. 12, No. 9, 1974, pp. 1198–1203. https://doi.org/10.2514/3.49453, URL https://doi.org/10.2514/3.49453.

[3] Sheppard, E., and Martinez-Sanchez, M., "Nonequilibrium ionization in plasma accelerators," *21st International Electric Propulsion Conference*, 1990. AIAA-1990-2608.

[4] Sheppard, E., and Martinez-Sanchez, M., "Analytical study on the influence of nonequilibrium ionization for current flow pattern and flow field of MPD arcjets," *21st International Electric Propulsion Conference*, 1990. AIAA-1990-2609.

[5] Sheppard, E., and Martinez-Sanchez, M., "Ionization Rate Models and Inlet Ignition in Self-Field MPD Thrusters," *23rd International Electric Propulsion Conference*, 1993. IEPC-93-071.

[6] Burton, R., and Tiliakos, N., "Injected propellant ionization in MPD thrusters," *28th Joint Propulsion Conference*, 1992. AIAA-1992-3295.

[7] Randolph, T., von Jaskowsky, W., Kelly, A., and Jahn, R., "Ionization Process in the Interelectrode Region of an MPD thruster," *22nd International Electric Propulsion Conference*, 1991. IEPC-1991-052.

[8] Randolph, T., von Jaskowsky, W., Kelly, A., and Jahn, R., "Measurement of Ionization Levels in the Interelectrode Region of an MPD Thruster," *28th Joint Propulsion Conference*, 1992. AIAA-1992-3460.

[9] Randolph, T. M., "Measurements of Ionization Levels in the Interelectrode Region of an MPD Thruster," Master's thesis, Princeton University, 1994.

[10] Abramov, V. A., Vinogradova, A. K., Dontsov, Y. P., Zavenyagin, Y. A., Kovrov, P. E., Kogan, V. I., and Morozov, A. I., "Investigation of Electron Temperature and Plasma Radiation in a Quasi-Stationary High-Current Discharge Between Coaxial Electrodes," *Proceedings of the 8th International Conference on Phenomena in Ionized Gases*, 1968. Panel 33.1.11, p. 160.

[11] Choueiri, E. Y., and Randolph, T. M., "Ionization Front in a High-current Gas Discharge," *Physics of Plasmas*, Vol. 14, 2007. https://doi.org/10.1063/1.2646365.

[12] Choueiri, E. Y., Kelly, A. J., and Jahn, R. G., "Current-driven plasma acceleration versus current-driven energy dissipation. Part II : Electromagnetic wave stability theory and experiments." *22nd International Electric Propulsion Conference*, 1991. IEPC-1991-100.

[13] Tilley, D. L., Choueiri, E. Y., Kelly, A. J., and Jahn, R. G., "Microinstabilities in a 10-kW Self-Field Magnetoplasmadynamic Thruster," *Journal of Propulsion and Power*, Vol. 12, No. 2, 1996.

[14] Choueiri, E. Y., "Anomalous Resistivity and Heating in Current-Drive Plasma Thrusters," *Physics of Plasmas*, Vol. 6, No. 5, 1999, pp. 2290–2306.

[15] Choueiri, E., "Instability of a current-carrying finite-beta collisional plasma." *Physical Review, E*, Vol. 64, No. 6, 2001, p. Article No. 066413.

[16] Choueiri, E. Y., Kelly, A. J., and Jahn, R. G., "MPD thruster instability studies," *19th International Electric Propulsion Conference*, 1987. AIAA-87-1067.

[17] Choueiri, E. Y., "An introduction to the plasma physics of the MPD thruster," *In the November/December Bimonthly Progress Report of the Electric Propulsion and Plasma Dynamics Laboratory.*, 1991. Technical Report MAE 1776.33.

[18] Polk, J. E., Kelly, A. J., and Jahn, R. G., "Characterization of cold cathode erosion processes," *20th International Electric Propulsion Conference*, 1988. AIAA-88-075.

[19] Hoskins, W. A., "Asymetric Discharge Patterns in the MPD Thruster," Master's thesis, Princeton University, 1990.

[20] Diamant, K. D., Choueiri, E. Y., and Jahn, R. G., "The role of spot mode transition in the anode fall of pulsed MPD thrusters," *24th International Electric Propulsion Conference*, 1995. IEPC-1995-234.

[21] Choueiri, E. Y., "The Scaling of Thrust in Self-Field Magnetoplasmadynamic Thrusters," *Journal of Propulsion and Power*, Vol. 14, No. 5, 1998, pp. 744–753. https://doi.org/10.2514/2.5337.

[22] Myers, R. M., "Energy Deposition in Low Power Coazial Plasma Thrusters," Ph.D. thesis, Princeton University, 1989.

[23] Tilley, D. L., "An Investigation of Microinstabilities in a kW Level Self-Field MPD Thruster," Ph.D. thesis, Princeton University, 1991.

[24] Uribarri, L., and Choueiri, E., "Creation of Onset Voltage Hash by Anode Spots in a Magnetoplasmadynamic Thruster," *Journal of Propulsion and Power*, Vol. 25, 2009, pp. 949–957.

[25] Rowe, R., von Jaskowsky, W., Clark, K., and Jahn, R., "Erosion Measurements on Quasisteady Magnetoplasmadynamic Thrusters," *Journal of Spacecraft and Rockets*, Vol. 19, No. 4, 1982, pp. 349–353.

[26] Turchi, P., Davis, J., and Roderick, N., *MPD Arcjet Thrust Chamber Flow Studies*, AIAA-90/2664, AIAA, 1990.

[27] Suckewer, S., "Excitation and ionization of atoms and ions in a non-thermal plasma. I. Populations of excited levels," *Journal of Physics B: Atomic and Molecular Physics*, Vol. 3, No. 3, 1970, pp. 380–389. https://doi.org/10.1088/0022-3700/3/3/010, URL https://doi.org/10.1088%2F0022-3700%2F3%2F3%2F010.

[28] Lochte-Holtgreven, W., *Plasma Diagnostics*, AVS Classics Series, AIP Press, 1995. URL https://books.google.com/books?id=dv1AAQAAIAAJ.

[29] Drawin, H. W., "Collision and transport cross-sections," , 1967.

[30] Kimura, A., Kobayashi, H., Nishida, M., and Valentin, P., "Calculation of collisional and radiative transition probabilities between excited argon levels," *Journal of Quantitative Spectroscopy and Radiative Transfer*, Vol. 34, No. 2, 1985, pp. 189 – 215. https://doi.org/https://doi.org/10.1016/0022-4073(85)90046-9, URL http://www.sciencedirect.com/science/article/pii/0022407385900469.

[31] Gomes, A. M., "Criteria for Partial LTE in an Argon Thermal Discharge at Atmospheric Pressure; Validity of the Spectroscopically Measured Electronic Temperature," *Journal of Physics D: Applied Physics*, Vol. 16, No. 3, 1983, pp. 357–378. https://doi.org/10.1088/0022-3727/16/3/019, URL https://doi.org/10.1088%2F0022-3727%2F16%2F3%2F019.

[32] Wiese, W. L., Brault, J. W., Danzmann, K., Helbig, V., and Kock, M., "Unified set of atomic transition probabilities for neutral argon," *Phys. Rev. A*, Vol. 39, 1989, pp. 2461–2471. https://doi.org/10.1103/PhysRevA.39.2461, URL https://link.aps.org/doi/10.1103/PhysRevA.39.2461.

[33] Wiese, W. L., Smith, M. W., and Miles, B. M., *Atomic transition probabilities. Vol. 2: Sodium through Calcium. A critical data compilation*, 1969.

[34] Hutchinson, I. H., *Principles of Plasma Diagnostics*, 2nd ed., Cambridge University Press, 2002. https://doi.org/10.1017/CBO9780511613630.